

## Spectral Correction and Dimensionality Reduction of Hyperspectral Images for Plant Water Stress Assessment

Lin Jian Wen<sup>1</sup>, Mohd Shahrime Mohd Asaari<sup>1\*</sup> and Stijn Dhondt<sup>2</sup>

<sup>1</sup>*School of Electrical and Electronic Engineering, Universiti Sains Malaysia, Nibong Tebal, 14300 USM, Penang, Malaysia*

<sup>2</sup>*Ghent University, Department of Plant Biotechnology and Bioinformatic, Ghent 9000, Belgium*

### ABSTRACT

Hyperspectral Imaging (HSI) is one of the emerging techniques used in plant phenotyping as it carries abundant information and is non-invasive to plants. However, factors like illumination effect and high-dimensional spectral features need to be solved to attain higher accuracy of plant trait analysis. This research explored and analysed spectral normalisation and dimensionality reduction methods. The focus of this paper is twofold; the first objective was to explore the Standard Normal Variate (SNV), Least Absolute Deviations (L1) and Least Squares (L2) normalisation for spectral correction. The second objective was to explore the feasibility of Principal Component Analysis (PCA) and Analysis of Variance Fisher's Test (ANOVA F-test) for spectral dimensionality reduction in spectral discriminative modelling. The analysis techniques were validated with HSI data of maize plants for early detection of water deficit stress response. Results showed that SNV performed the best among the three normalisation methods. Besides, ANOVA F-test outperformed PCA for the band selection method as it improved the trait assessment on the water deficit response of maize plants.

*Keywords:* Analysis of variance fisher's test, hyperspectral imaging, plant phenotyping, principal component analysis, standard normal variate

### ARTICLE INFO

#### Article history:

Received: 14 July 2022

Accepted: 05 October 2022

Published: 25 May 2023

DOI: <https://doi.org/10.47836/pjst.31.4.13>

#### E-mail addresses:

[jianwenapp1996@gmail.com](mailto:jianwenapp1996@gmail.com) (Lin Jian Wen)

[mohdshahrime@usm.my](mailto:mohdshahrime@usm.my) (Mohd Shahrime Mohd Asaari)

[stdho@psb.vib-ugent.be](mailto:stdho@psb.vib-ugent.be) (Stijn Dhondt)

\*Corresponding author

### INTRODUCTION

The advanced technology in plant genomics is important for breeding more sustainable crops. However, the ability to dissect traits' genetics depends on plant phenotyping development. Among the techniques developed for plant phenotyping are visible,

fluorescence imaging, infrared imaging, hyperspectral Imaging (HSI), and 3D structural tomography.

Visible imaging was performed to plant phenotyping by analysing digital images with spectral information from 400 nm–700 nm. The advantage of this technique is low implementation cost and maintenance fee. Despite that, there are limitations like restricted analysis of plant physiology and difficulty caused by overlapping leaves. Fluorescence imaging contradicts visible imaging by detecting fluorescence signals (250 nm–700 nm) emitted from plants after exposure to visible or UV light. This method detects plant diseases (Balachandran et al., 1997; Lohaus et al., 2000). In general, every object emits infrared radiation, allowing infrared imaging possible for plant phenotyping (Kastberger & Stachl, 2003). Infrared radiation ranges from 700 nm to 1000 nm. The wide range will require a high computational cost. Therefore, many implementations of infrared imaging only focus on a certain band range. For instance, thermal imaging utilises spectra from 3–5  $\mu\text{m}$  and 7–14  $\mu\text{m}$  for detecting biotic and abiotic stresses (Chaerle & van der Straeten, 2000; Nilsson, 1995). Near-infrared (NIR) is another way to utilise infrared radiation. It ranges from 700 nm–1400 nm and has a higher reflective intensity on healthy green plants (Yang et al., 2013). The benefit of NIR imaging is that radiation can be transmitted through leaves that overcome difficulties visible imaging faces.

Hyperspectral imaging (HSI) is a technique that combines both visible and NIR imaging methods. The downside of visible and NIR imaging can be overcome mutually. Furthermore, HSI can divide images into bands, enabling analysis of the plant's condition using Vegetation Indices (VI). Ihuoma and Madramootoo (2019) compared a few vegetation indices extracted from hyperspectral images to monitor the water stress level in tomato plants and found that Water Index (WI), Photochemical Reflectance Index centred at 550 nm (PRI550), and Optimised Soil Adjusted Vegetation Index (OSAVI) are the most sensitive indices in distinguishing plants with 80% or less available water content (AWC). Besides, the popular NDVI and RENDVI were studied by Andaryani et al. (2019) to investigate the drought level in the agriculture field. These studies show that water-sensitive VIs can detect drought stress to a certain extent. However, these studies do not consider linearity and scattering of illumination. Thus, solely computing VIs from hyperspectral data might not be the most optimum method for identifying water-stressed plants. In different studies, HSI has been used to estimate leaf water content (LWC) and the result is compared with LWC value measured destructively (Ge et al., 2016; Pandey et al., 2017). However, this approach is undesirable as many samples will be destroyed for long-duration studies. In contrast, the comparison is made between hyperspectral images of the control and water-deficit groups (Asaari et al., 2019) by computing the Euclidean Distance (ED) of the hyperspectral spectrum with reference from the control group.

Although HSI has many edges over other imaging techniques, it is still far from perfection. The illumination effect is still one of the difficulties faced by plant phenotyping.

Besides, the high dimension of hyperspectral images also leads to high computational costs. This study performs quantitative analysis for eliminating the illumination effect using SNV, L1, and L2 normalisation techniques to tackle these concerns. SNV is considered the effective method to reduce the illumination effect (Asaari et al., 2018). Even though SNV shows prominent results in mitigating linear illumination effect (Mohd Asaari et al., 2018; Vigneau et al., 2011). One of the downsides is the inability to extract VIs from SNV spectra as the values are not bounded in the positive range, thus preventing direct linkage between the normalised wavelength and the biophysical properties of the plant. It is worth mentioning that, apart from SNV, Savitzky-Golay (SG) filter (Fletcher & Turley, 2018; Liu et al., 2019) and Multiple Scattering Correction (MSC) (Geladi et al., 1985; Isaksson & Næs, 1988) are other popular spectral pre-treatment methods. SNV and MSC are both spectral pre-processing inspired by chemometrics. The difference between SNV and MSC is that MSC requires a reference spectrum deemed unaffected by noises (Li et al., 2018). In most HSI analyses, the performance of MSC is very dependent on the average spectrum as it is used as the reference spectrum, which is difficult to excess, especially on articulated plant structures. In this context, SNV performs better than MSC (Mishra, Lohumi, et al., 2020) as the average spectrum is not out of the noise. On the other hand, the SG filter is used to smoothen hyperspectral data from the data aspect without considering chemometrics. Thus, pure smoothing ignores the multiplicative and additive effect when illumination is reflected from the plant surface.

Another popular method in pre-processing of hyperspectral data is L1 and L2. In a recent study (Zhuang & Ng, 2020), L1 normalisation was used to remove Gaussian noise from hyperspectral images. On the other hand, Feng et al. (2022) used L2 normalisation to improve feature robustness towards impulse noise before feeding data into the deep learning model. Even though these studies show satisfactory results for respective objectives, the data used are remote sensing hyperspectral images. To the author's knowledge, no study has been done using L1 and L2 normalisation on proximal hyperspectral images thus far. In recent work (Abenina et al., 2022), HSI analysis was performed to study plant traits by comparing the SG filter, MSC and SNV. The results showed that SNV performs best among all. Thus, only SNV is implemented here to compare with L1 and L2 to see if the proposed normalisation method works better than the current best method.

Besides the illumination issues, another common difficulties researchers face when dealing with a hyperspectral image is the curse of dimensionality, also known as Hughes Phenomenon (Hughes, 1968). The high number of bands carried by hyperspectral images always requires high computational power and time for analysis. To tackle these concerns, two dimension reduction methods, PCA and ANOVA F-test (Asaari et al., 2019; Calzone et al., 2021; Pandey et al., 2017), are explored to quantify their feasibility for improving spectral discrimination. Even though these two methods serve the same purpose, the

dimensionally reduced data characteristic differs. Principal Components (PCs) generated by PCA are non-interpretable, whereas ANOVA F-test works more directly by selecting the most varied bands. This study compares the effectiveness of the two methods in dimension reduction and determines if they can be used as an alternative to each other.

This study aims to address two objectives. The first objective involves evaluating the suitability of two proposed normalization methods, L1 and L2 in comparison to the current best method, SNV normalization, for HSI analysis. The second objective entails comparing the water stress detection efficiency of two dimension reduction methods, namely PCA and ANOVA F-test. The more effective normalization and dimension reduction method will be determined via computation of Euclidean Distance (ED) between spectra of two different groups of maize plants; healthy and water deficit groups.

## METHODOLOGY

In this work, the images of maize plants were obtained from Asaari et al. (2018), in which imaging was done in the VIB-UGent Center greenhouse in Ghent, Belgium. Pushbroom hyperspectral camera with visible to NIR detection range was coupled with an array of 3x3 halogen lamps, each placed at the same level as the camera. During image acquisition, maize plants were transferred via a high-throughput phenotyping platform (HTPPP) and individually snapped in dedicated enclosed cabins.

The obtained data were separated into two sets, where the first dataset contains hyperspectral images of five maize plants captured at five different platform heights. Meanwhile, the second dataset contains hyperspectral images of ten maize plants, categorised into control and water-deficit groups, followed consecutively for nine days. Hyperspectral images captured have resolutions of 510 x 328 pixels, and each pixel has 194 spectral bands ranging from 400 nm to 1000 nm.

After the images dataset was prepared, white and dark reference was carried out to convert reflectance intensities into values between 0 and 1 followed by removal of bands with inconsistent values. After that, vegetation pixels were segmented by calculating every pixel's Normalised Difference Vegetation Index (NDVI). Pixels with NDVI values lower than 0.3 were removed.

To achieve the first objective spectral normalisation was performed after the pre-processing steps to reduce the illumination effects. SNV, L1, and L2 normalisations were carried out separately on both datasets. For the first dataset, clustering was used to classify normalised spectra into clusters. Five graphs representing different platform heights were studied for each spectra type. For the second dataset, spectra similarity measurement was computed between the mean spectra of maize plants and daily reference. Results were presented in error bar graphs to determine the duration for complete discrimination between control and water-deficit groups. In achieving the second objective, the normalised

spectra of the second dataset were further processed by dimension reduction using PCA and ANOVA F-test separately. Then, spectra similarity measurement was performed again to determine the duration of attaining the complete separation of control and water-deficit groups. Figures 1 and 2 show the flowchart from image acquisition to plant discrimination.

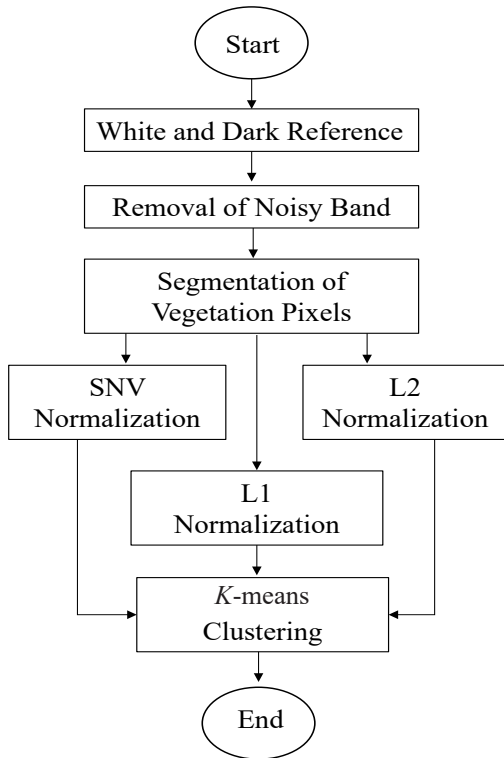


Figure 1. Process flow for the first dataset

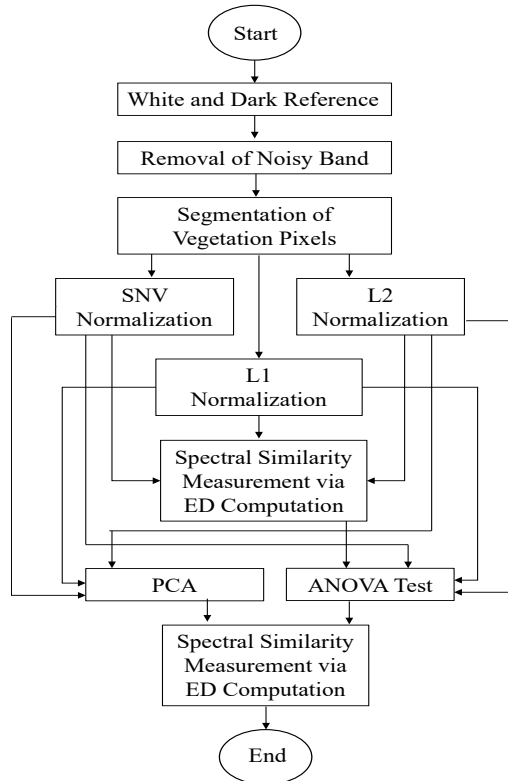


Figure 2. Process flow for the second dataset

**Image Pre-processing**

There were three steps in this stage. The first was a white and dark reference, a standardisation method common in hyperspectral images study (Geladi et al., 2004; Ortaç et al., 2016; Shaikh et al., 2021). White reference is obtained by capturing an image when placing a high reflectance (~99%) board perpendicularly opposite the camera. On the other hand, dark reference is the image captured when the shutter or light is off. Reflectance was calculated using Equation 1:

$$R = \frac{I-D}{W-D} \tag{1}$$

where  $R$  is reflectance,  $I$  is original image intensity,  $D$  is a dark reference, and  $W$  is a white reference.

Noisy bands fluctuate inconsistently due to different kinds of noise like thermal, instrumental, and photon noise, thus containing more outlying values. In this work, the bands below 500 nm and above 810 nm are visibly noisy and were removed, leaving spectra with 111 spectral bands after the process.

Since leaves of maize plants did not just form the original hyperspectral image but also unnecessary components like pots and platforms, segmentation of vegetation pixels was required. NDVIs of all pixels were calculated. Then, the threshold was set to 0.3. It means pixels with NDVI of more than 0.3 were deemed to belong to the maize plant's leaves. Therefore, only leaves remain for further analysis after segmentation.

### Spectral Normalisation

After the above pre-processing steps, normalisation was needed to reduce the illumination effect. The ideal intensity of light received was when the whole object's surface was perpendicular to the sensor. However, in real life, the leaves of maize plants face different directions. In addition, leaf surfaces were not smooth, causing light to scatter in all directions.

When doing vector (L1 and L2) normalisation, all spectra were treated as vectors with values of all bands as components. Equations 2 and 3 are norm computations for L1 and L2, respectively. Vector normalisation changed the spectrum into a unit vector by Equation 4, and only the magnitude of the spectrum was transformed. All normalised spectra had uniform magnitude, thus minimising the illumination effect.

$$norm = |s_1| + |s_2| + \dots + |s_N| \tag{2}$$

$$norm = \sqrt{s_1^2 + s_2^2 + \dots + s_N^2} \tag{3}$$

$$(s_i)_{normalized} = \frac{s_i}{norm} \tag{4}$$

Other than vector normalisation, SNV normalisation was also applied in this research to compare the performances of different normalisation methods. SNV normalisation has been implemented in recent hyperspectral studies (Abenina et al., 2022; Mishra et al., 2020; Polder, et al., 2020) and is deemed the effective way to mitigate the scattering effect. It is aimed to transform the spectrum to have a mean of 0 and a standard deviation of 1 using Equation 5:

$$(X_i)_{SNV} = \frac{X_i - \bar{X}_i}{\sigma_i} \tag{5}$$

where  $\bar{X}_i$  is the mean, and  $\sigma_i$  is the standard deviation of data, respectively.

The noise on received spectra can be illustrated as Equation 6, where  $s_{reference}(\lambda)$  is said to be light reflectance at a reference. Besides,  $\beta$  refers to the illumination effect caused by the inclination of leaves and the distance between the camera and the maize plant. Moreover,  $\alpha$  refers to specular reflectance, the additive effect on the reference spectrum.

$$s_{reference}(\lambda) = \beta \cdot s_{reference}(\lambda) + \alpha \quad (6)$$

By some rearrangement, Equation 7 was obtained. By comparing Equations 5 and 7, it was not hard to notice that  $\alpha$  refers to the spectrum mean, and  $\beta$  refers to the standard deviation. Therefore, from this theory, SNV normalisation can be used to yield noiseless spectra.

$$s_{reference}(\lambda) = \frac{s_{received}(\lambda) - \alpha}{\beta} \quad (7)$$

### Spectral Discrimination

The classification was performed on normalised spectra to determine if a spectra type has high efficiency in water stress detection. For the first dataset, the classification method performed was  $k$ -means clustering (Ranjan et al., 2017). Built-in  $k$ -means function was used, and the algorithm takes in a few parameters: the number of clusters ( $k$ ) and maximum iterations. After referring to (Asaari et al., 2019), the  $k$  value was set to 6. Maximum iteration was set to 500 as well to prevent the infinite running of code. A bar graph with the number of pixels in each cluster was presented for each platform height. The variation across different bar graphs was studied to see if platform heights affect normalisation performance.

For the second normalised dataset, spectra similarity was measured between daily reference and mean spectrum of each maize plant by calculating the ED between them. The formula for ED is shown in Equation 8. After the ED was computed, the daily mean and standard deviation were calculated from the daily ED obtained according to control and water-deficit groups. Then, the result was shown as error bar graphs in which no overlapping of the error bar indicates complete discrimination of maize plants experiencing water stress.

$$ED(q, r) = \sqrt{\sum_{\lambda=1}^B (q(\lambda) - r(\lambda))^2} \quad (8)$$

### Dimensionality Reduction

In this work, each hyperspectral image has around 10000 vegetation pixels, and each pixel has 111 bands. The computational cost was very high for such a large amount of data. Therefore, PCA and ANOVA F-test were applied on the normalised second dataset to see if improvement in the duration of water stress detection happened after the spectra dimension was reduced.

Each day's plant was represented by its mean spectrum when implementing PCA. Besides, the daily reference spectrum will also be computed for the control and water-deficit groups. All these spectra will be combined as samples for PCA. There are a total of 108 rows with 111 columns. In MATLAB, PCA was applied using the built-in PCA function. The first few PCs were used to check the effect of PCA.

In this work, the spectral band used for analysis was from 400 nm to 810 nm with a bandwidth of 3.1 nm. Even though information can be extracted from every band, not all bands contributed the same to water stress detection. ANOVA F-test uses the average daily spectrum as input. The built-in function, `anova1`, was used to compute the daily F-value for each band. Bands with the highest 10% of F-value were elected for each day. The selected bands were used for spectra similarity measurement to determine the duration taken for discrimination between control and water-deficit groups.

## RESULTS AND DISCUSSION

The effect of SNV, L1, and L2 normalisation on different platform heights was evaluated to satisfy the first objective. *K*-means clustering was used to segregate results into different clusters displayed in the bar graph. Besides, the outcome of water stress detection using different spectra types was evaluated by calculating ED between spectra. The error bar was displayed for all nine days of the experiment. However, only the first seven days were studied for water stress detection as maize plants in the water-deficit group were not irrigated in these seven days.

PCA and ANOVA F-test were applied on normalised spectra separately to realise the second objective. Then, spectra similarity measurement with ED has performed again on the dimensionally reduced data. The same procedure of water stress analysis for the first objective was done again to determine the effect of each dimension reduction method.

### Image Processing

Figure 3 shows spectra where bands below 500 nm and above 810 nm were removed. The variance of spectra decreases from 500 nm to around 650 nm, and after 700 nm, the variance of spectra increases and remains constant after around 750 nm. The number of spectral involved is 111, with 3.1 nm as the width of each band.

Figures 4 and 5 show the hyperspectral image before and after segmentation using threshold NDVI of 0.3, as stated in (Gandhi et al., 2015) as best for vegetation analysis. Figure 4's image background includes soil, pots, and a platform base. Therefore, the NDVI of these pixels will be lower than 0.3, representing non-vegetative pixels. The remaining spectra are around 10000 pixels for each maize plant, as shown in Figure 5. These pixels will be considered for further analysis.

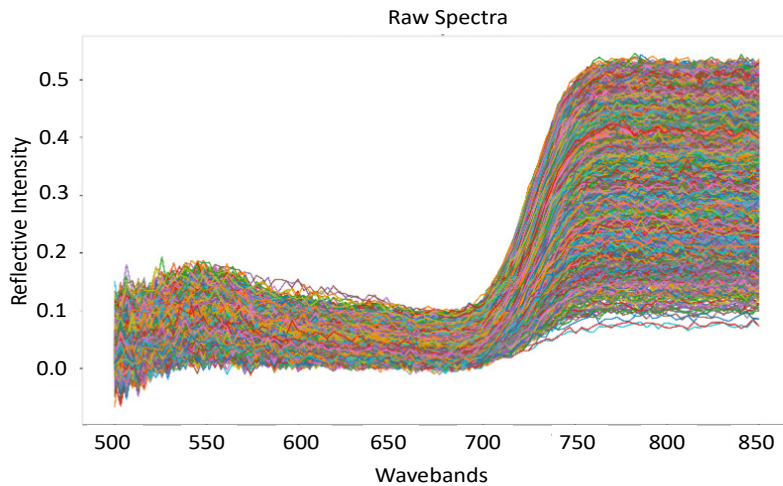


Figure 3. Spectra after removal of noisy bands



Figure 4. Hyperspectral image presented in RGB



Figure 5. Hyperspectral image after segmentation

### Analysis of Spectral Normalisation of HSI of Maize Plant at Different Imaging Platform Heights

After normalisation using SNV, L1, and L2, the normalised spectra underwent classification using *k*-means clustering to determine if normalisation performs differently according to platform heights. MATLAB built-in *k*-means function has a parameter of 6 as the *k* value and 500 as the maximum iteration. Results of *k*-means clustering on SNV, L1, and L2 spectra are shown in Figures 6, 7, and 8, respectively. From Figures 6 and 8, it is observed that cluster 5 and 6 has the greatest number of pixels. Figure 7 shows that most pixels belong to clusters 3, 4, and 5. Besides, the graph pattern is consistent across four heights for all three spectrum types. It proves normalisation has consistent efficiency from 0 mm to 450 mm platform heights. The findings align with the study conducted by (Witteveen et al., 2022), which also observed normalization is not impacted by variations in distance.

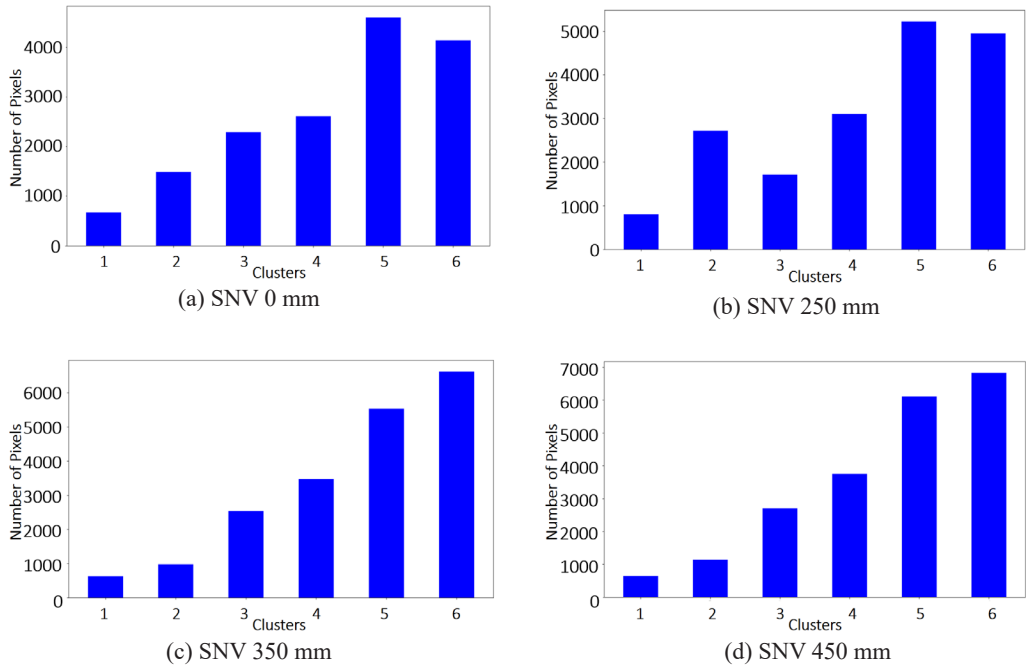


Figure 6. K-means clusters shown in the bar graph for SNV normalised spectra at different imaging platforms: (a) 0 mm, (b) 250 mm, (c) 350 mm, and (d) 450 mm

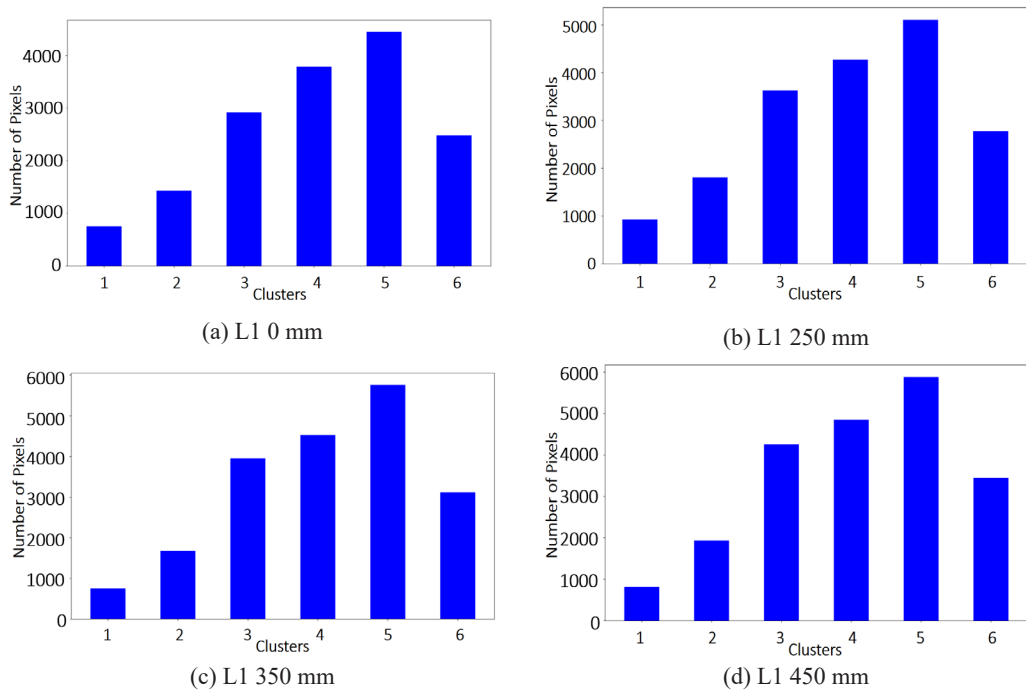


Figure 7. K-means clusters shown in the bar graph for L1 normalised spectra at different imaging platforms: (a) 0 mm, (b) 250 mm, (c) 350 mm, and (d) 450 mm

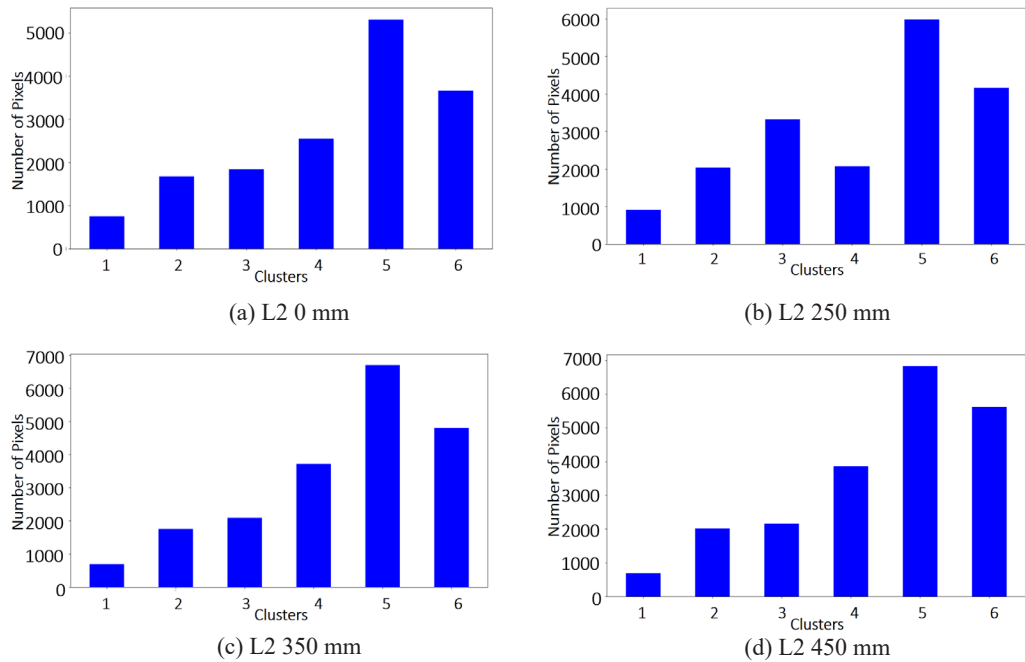


Figure 8. K-means clusters shown in the bar graph for L2 normalised spectra at different imaging platforms: (a) 0 mm, (b) 250 mm, (c) 350 mm, and (d) 450 mm

### Analysis of Spectral Normalisation on Water Deficit Response in Maize Plants

After proving that normalisation works the same at different platform heights, spectra similarity measurement was performed for raw, SNV, L1, and L2 normalised spectra. Daily reference was first computed by getting the mean of maize plants in the control group. Then, the ED between the mean spectrum of maize plants and daily reference was calculated. Daily ED values were categorised according to control and water-deficit groups. Then, daily mean and standard deviation were obtained from these ED values and presented in an error bar graph. Note that in this study, no Cross-Validation (CV) is performed as only computation of ED between mean reference spectrum is done without any parameter tuning required. CV is generally used when developing a machine learning model, which requires the dataset to be split into training and testing sets. After the CV's k-folds are performed, each fold's parameter will be averaged and used as model parameters. In the ED calculation, the error bars' lower and upper boundaries represent the minimum and maximum of each sample group, respectively. Thus, the complete separation of the error bar is sufficient to indicate drought plants among samples.

From Figure 9(a), error bar analysis similar to (Asaari et al., 2019) has been conducted. The duration taken for raw spectra to separate control and water-deficit groups is 7 days, while for SNV spectra, it takes 4 days. On the contrary, both vector normalisations, L1 and

L2, fail to detect maize plants experiencing water stress within the first 7 days. It can be noticed that the red error bar, which represents the difference between water-deficit maize plants and daily reference, increases consistently from day 2 to day 7 for SNV. It shows that SNV-normalised spectra respond according to the plant’s water level. However, a closer observation of Figure 9 (c-d) shows an unusually large increment of the control error bars from day 4 to day 6. It causes the error bar of both groups to “stick” with each other and not be able to discriminate in the first 7 days completely. Therefore, from Figure 9, it can be concluded that spectra after being SNV normalised are better compared to L1 and L2 normalised spectra in detecting water deficit stress response in maize plants.

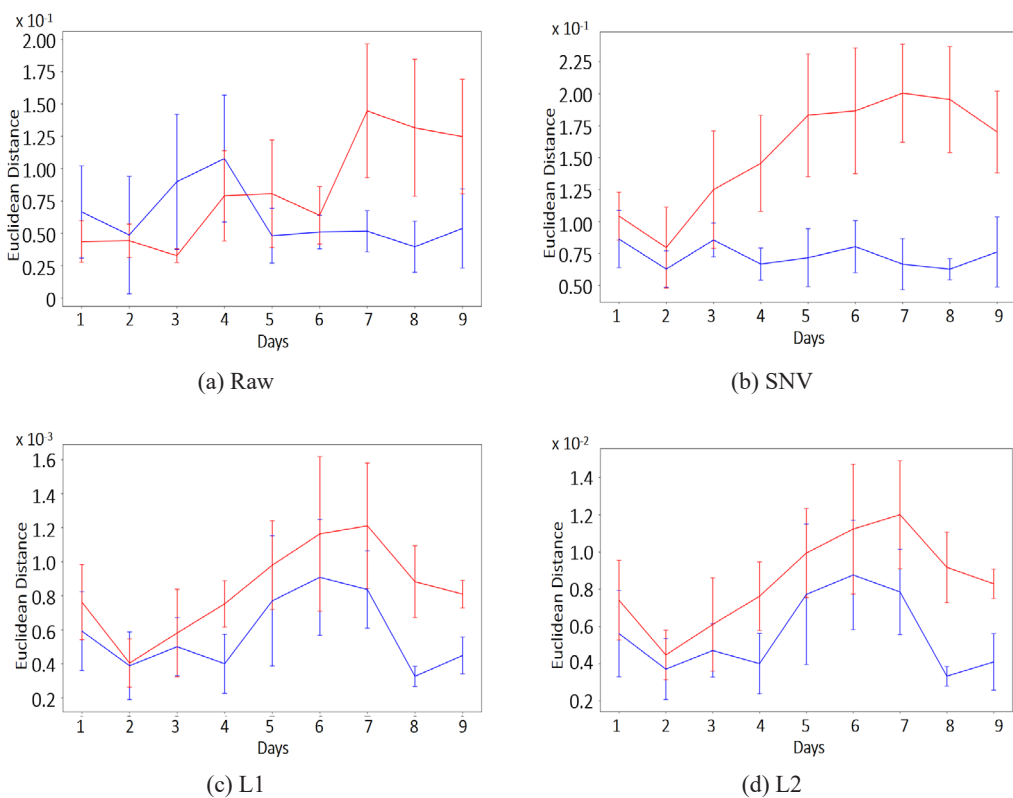


Figure 9. Spectra similarity result on (a) raw, (b) SNV, (c) L1 and (d) L2 spectra with blue error bar representing the control group and red error bar representing the water deficit group.

### Analysis of Dimensionality Reduction

The second objective of this work studies the effect of dimension reduction methods, PCA and ANOVA F-test in water stress detection. Both methods have different ways of implementation. However, they serve the same purpose: to reduce the computational cost of analysis.

Results of spectra similarity measurement after PCA is applied and shown in Figures 10 and 11 for each spectra type when 1 and 10 PCs were selected. When comparing with Figure 9, graphs with 10 PCs are very similar to the spectra similarity result before dimension reduction. On the other hand, graphs using only 1 PC show worse results when compared with spectra similarity results before dimension reduction. Therefore, it can be deduced that PCA does not affect the duration taken for water stress detection when enough PCs are used. A closer look at Figure 10 shows that when 1 PC is used for spectra similarity measurement, the result is not as good as another two. It is due to the variance in the first PC being insufficient “replicate” that of the whole data set. Similar scenarios have been observed in studies conducted by (Fernández et al., 2022; Ren et al., 2020; Vu et al., 2016) where multiple PCs were utilized for machine learning computation. Therefore, the optimum number of PCs used in this work is 10.

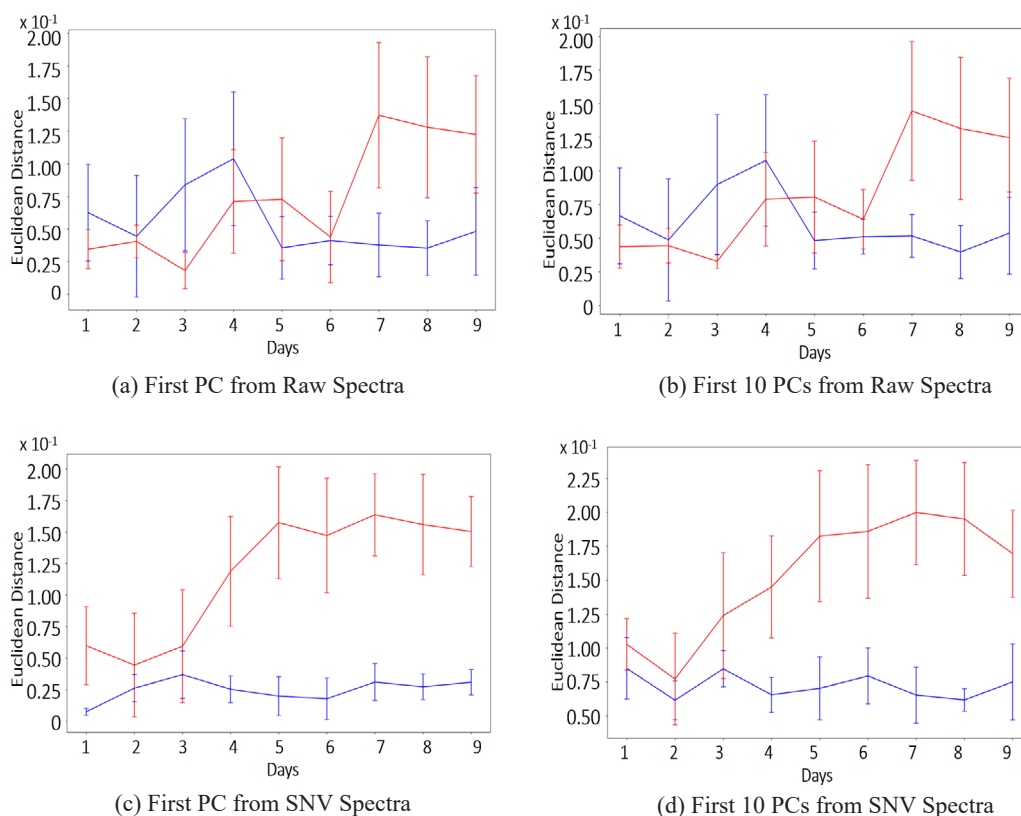


Figure 10. Spectra similarity result-based PCA with 1 and 10 PCs of raw spectra (a-b) and 1 and 10 PCs of SNV normalised spectra (c-d). The blue error bar represents the control group, and the red represents the water deficit group.

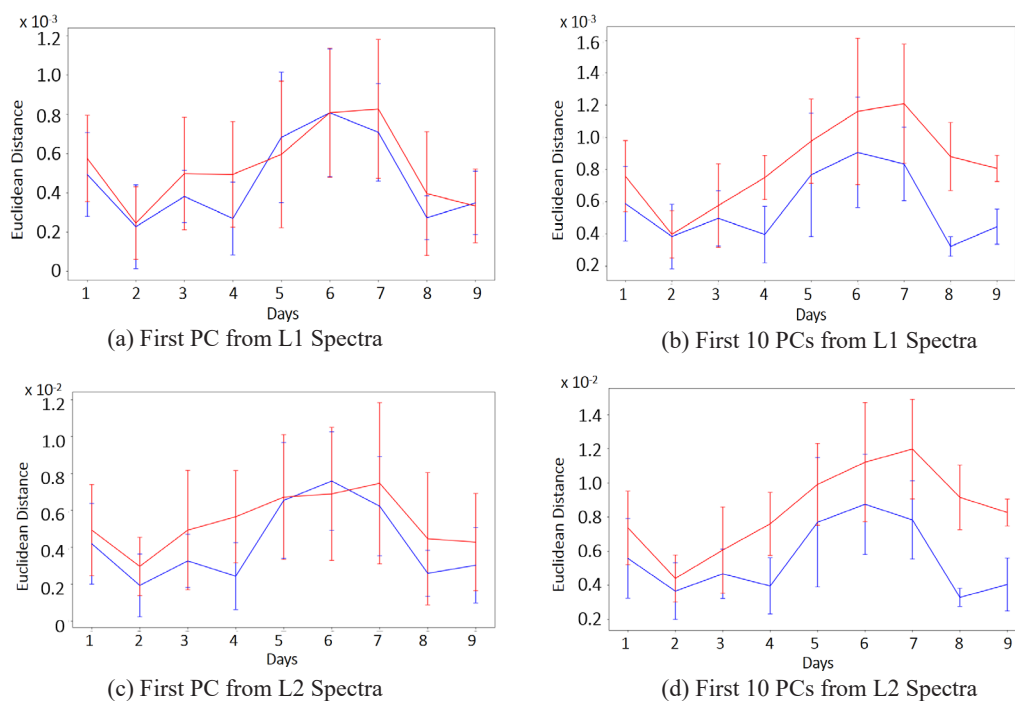


Figure 11. Spectra similarity based on PCA with 1 and 10 PCs of L1 normalised spectra (a-b) and 1 and 10 PCs of L2 normalised spectra. The blue error bar represents the control group, and the red represents the water deficit group.

Spectra, which have been dimensionally reduced using ANOVA F-test, were processed with the same spectra similarity measurement method used for objective one. Results for raw, SNV, L1, and L2 spectra are shown in Figure 12. Improvement happens for all normalised spectrum types when comparing these results with the spectral discrimination in Figure 9. For SNV spectra, the duration taken for water stress detection was reduced from 4 days to just 4 days. Besides, even though the result on L1 spectra shows that water stress detection still fails in the first 7 days, a further separation between error bars can be observed. Different from L1 to L2 spectra show the successful separation of control and water deficit on the fourth day. The improvement from failure to success in just 4 days for water stress detection gives ANOVA F-test the highest efficiency when applied to L2 spectra. From the results from PCA and ANOVA F-test, it can be deduced that ANOVA F-test works better in improving the performance of HSI analysis in terms of duration to detect water-deficit maize plants. Conversely, PCA can reduce the computational cost, but it does not affect the result of water stress detection.

A comparison was made with several well-known vegetation indices as used in the previous studies to quantify the effectiveness of the analysis method of HSI performed in this study for the use case of early drought stress detection in the plant (Andaryani et al.,

2019; Ihuoma & Madramootoo, 2019). Figure 13 shows the result of separating samples from control and drought groups using NDVI, OSAVI, PRI 550 and RENDVI. All four VIs considered sensitive to water content cannot distinguish drought plants completely from the control group throughout the 9 days of the experiment. It further highlights the importance of normalisation to minimise collinear and scattering effects before analysis.

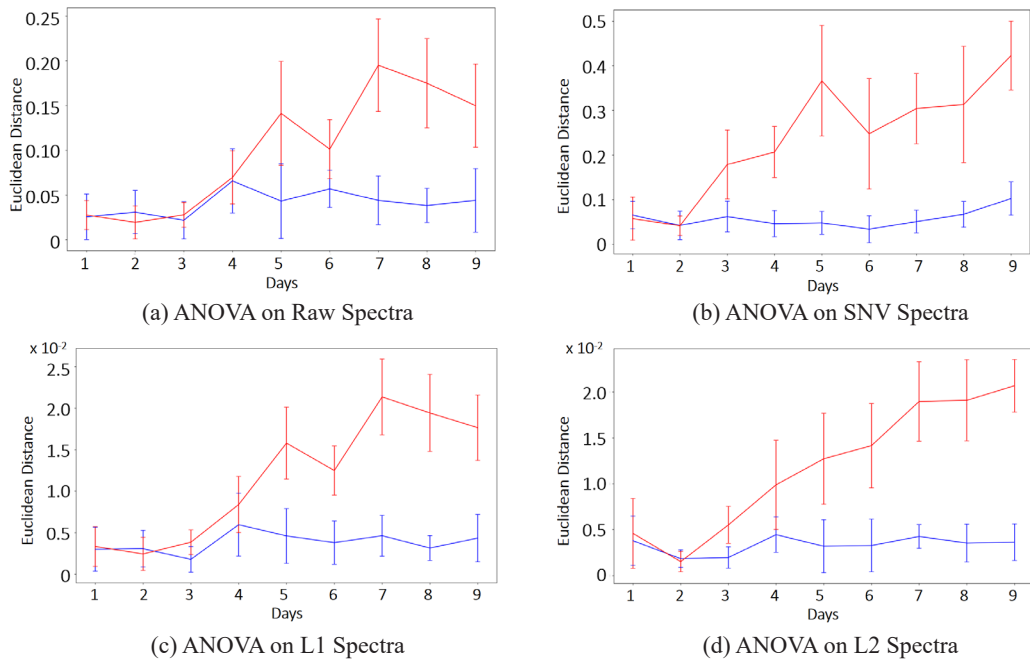


Figure 12. Spectra similarity result on (a) raw (b) SNV (c) L1 and (d) L2 spectra after performing ANOVA F-test with blue error bar representing the control group and red error bar representing water deficit group.

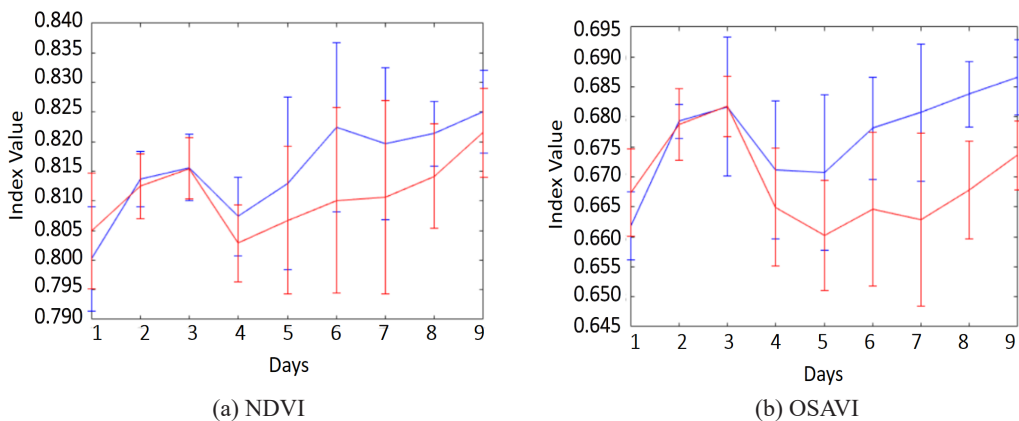


Figure 13. Vegetation indices value (a) NDVI, (b) OSAVI, (c) PRI 550 and (d) RENDVI for drought plants detection on raw spectra.

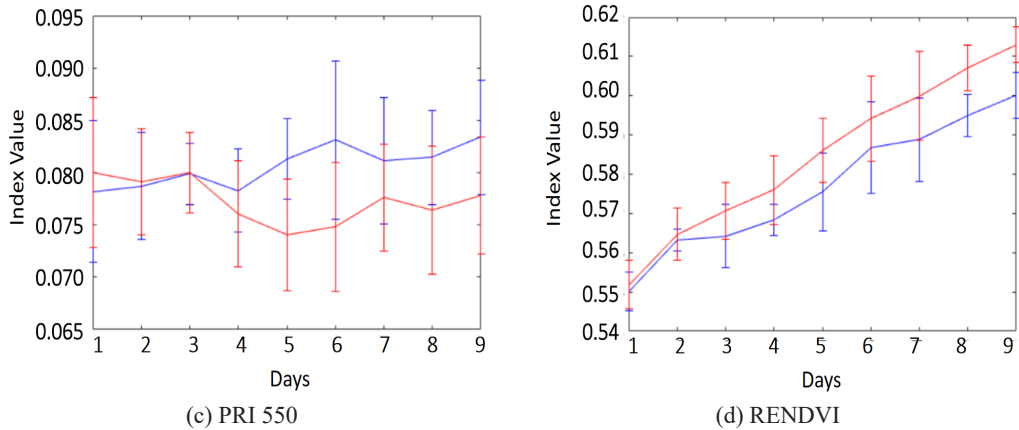


Figure 13. Continue

## CONCLUSION

In this paper, two comparisons have been carried out: the performances between the effect of SNV, L1, and L2 normalisation and between PCA and ANOVA F-test in water stress detection. The first objective was achieved with spectra similarity measurement performed on SNV spectra which successfully separated control and water-deficit groups in 4 days, while L1 and L2 spectra showed failure in water stress detection. Furthermore, the second objective was achieved by showing that similarity measurement on spectra after treatment using ANOVA F-test showed better performance in water stress detection. On the other hand, spectra similarity measurement after PCA showed the same result as in the non-dimensionally reduced one.

## ACKNOWLEDGMENTS

The authors acknowledged the Ministry of Higher Education (MOHE) Malaysia for the Fundamental Research Grant Scheme with Project Code: FRGS/1/2020/TK0/USM/02/13. The author also fully acknowledged the VIB-UGent Center for Plant Systems Biology of Ghent University Belgium research team for help in preparing the Hyperspectral images.

## REFERENCES

- Abenina, M. I. A., Maja, J. M., Cutulle, M., Melgar, J. C., & Liu, H. (2022). Prediction of potassium in peach leaves using hyperspectral imaging and multivariate analysis. *AgriEngineering*, 4(2), 400-413. <https://doi.org/10.3390/agriengineering4020027>
- Andaryani, S., Trolle, D., & Asl, A. M. (2019). *Application of hyperion data for investigating agriculture field stress to drought conditions*. EasyChair.

- Asaari, M. S. M., Mishra, P., Mertens, S., Dhondt, S., Inzé, D., Wuyts, N., & Scheunders, P. (2018). Close-range hyperspectral image analysis for the early detection of stress responses in individual plants in a high-throughput phenotyping platform. *ISPRS Journal of Photogrammetry and Remote Sensing*, *138*, 121-138. <https://doi.org/10.1016/j.isprsjprs.2018.02.003>
- Asaari, M. S. M., Mertens, S., Dhondt, S., Inzé, D., Wuyts, N., & Scheunders, P. (2019). Analysis of hyperspectral images for detection of drought stress and recovery in maize plants in a high-throughput phenotyping platform. *Computers and Electronics in Agriculture*, *162*, 749-758. <https://doi.org/10.1016/j.compag.2019.05.018>
- Balachandran, S., Hurry, V. M., Kelley, S. E., Osmond, C. B., Robinson, S. A., Rohozinski, J., Seaton, G. G. R., & Sims, D. A. (1997). Concepts of plant biotic stress. Some insights into the stress physiology of virus-infected plants, from the perspective of photosynthesis. *Physiologia Plantarum*, *100*(2), 203-213. <https://doi.org/10.1111/j.1399-3054.1997.tb04776.x>
- Behmann, J., Steinrücken, J., & Plümer, L. (2014). Detection of early plant stress responses in hyperspectral images. *ISPRS Journal of Photogrammetry and Remote Sensing*, *93*, 98-111. <https://doi.org/10.1016/j.isprsjprs.2014.03.016>
- Calzone, A., Cotrozzi, L., Lorenzini, G., Nali, C., & Pellegrini, E. (2021). Hyperspectral detection and monitoring of salt stress in pomegranate cultivars. *Agronomy*, *11*(6). <https://doi.org/10.3390/agronomy11061038>
- Chaerle, L., & van der Straeten, D. (2000). Imaging techniques and the early detection of plant stress. *Trends in Plant Science*, *5*(11), 495-501. [https://doi.org/10.1016/S1360-1385\(00\)01781-7](https://doi.org/10.1016/S1360-1385(00)01781-7)
- Feng, F., Zhang, Y., Zhang, J., & Liu, B. (2022). Small sample hyperspectral image classification based on cascade fusion of mixed spatial-spectral features and second-order pooling. *Remote Sensing*, *14*(3), Article 505. <https://doi.org/10.3390/rs14030505>
- Fernández, C. I., Leblon, B., Wang, J., Haddadi, A., & Wang, K. (2022). Cucumber powdery mildew detection using hyperspectral data. *Canadian Journal of Plant Science*, *102*(1), 20–32. <https://doi.org/10.1139/cjps-2021-0148>
- Fletcher, R. S., & Turley, R. B. (2018). Comparing Canopy Hyperspectral Reflectance Properties of Palmer amaranth and Okra and Super-Okra Leaf Cotton. *American Journal of Plant Sciences*, *09*(13), 2708–2718. <https://doi.org/10.4236/ajps.2018.913197>
- Gandhi, G. M., Parthiban, S., Thummalu, N., & Christy, A. (2015). Ndvi: Vegetation Change Detection Using Remote Sensing and Gis – A Case Study of Vellore District. *Procedia Computer Science*, *57*, 1199–1210. <https://doi.org/10.1016/j.procs.2015.07.415>
- Ge, Y., Bai, G., Stoerger, V., & Schnable, J. C. (2016). Temporal dynamics of maize plant growth, water use, and leaf water content using automated high throughput RGB and hyperspectral imaging. *Computers and Electronics in Agriculture*, *127*, 625-632. <https://doi.org/10.1016/j.compag.2016.07.028>
- Geladi, P., Burger, J., & Lestander, T. (2004). Hyperspectral imaging: Calibration problems and solutions. *Chemometrics and Intelligent Laboratory Systems*, *72*(2), 209-217. <https://doi.org/10.1016/j.chemolab.2004.01.023>
- Hughes, G. F. (1968). On the mean accuracy of statistical pattern recognizers. *IEEE Transactions on Information Theory*, *14*(1), 55-63. <https://doi.org/10.1109/TIT.1968.1054102>

- Ihuoma, S. O., & Madramootoo, C. A. (2019). Sensitivity of spectral vegetation indices for monitoring water stress in tomato plants. *Computers and Electronics in Agriculture*, *163*, Article 104860. <https://doi.org/10.1016/j.compag.2019.104860>
- Isaksson, T., & Næs, T. (1988). The Effect of Multiplicative Scatter Correction (MSC) and Linearity Improvement in NIR Spectroscopy. *Applied Spectroscopy*, *42*(7), 1273–1284. <https://doi.org/10.1366/0003702884429869>
- Kastberger, G. & Stachl, R. (2003). Infrared imaging technology and biological applications. *Behaviour Research Methods, Instruments & Computers*, *35*(3), 429-439. <https://doi.org/10.3758/BF03195520>
- Li, X., Li, R., Mengyu Wang, Liu, Y., Zhang, B., & Zhou, J. (2018). Hyperspectral Imaging and Their Applications in the Nondestructive Quality Assessment of Fruits and Vegetables. *Hyperspectral Imaging in Agriculture, Food and Environment*, 28–63. <https://doi.org/10.1016/j.colsurfa.2011.12.014>
- Liu, J., Han, J., Chen, X., Shi, L., & Zhang, L. (2019). Nondestructive detection of rape leaf chlorophyll level based on Vis-NIR spectroscopy. *Spectrochimica Acta Part A: Molecular and Biomolecular Spectroscopy*, *222*, 117202. <https://doi.org/10.1016/j.saa.2019.117202>
- Lohaus, G., Heldt, H. W., & Osmond, C. B. (2000). Infection with phloem limited abutilon mosaic virus causes localized carbohydrate accumulation in leaves of abutilon striatum: relationships to symptom development and effects on chlorophyll fluorescence quenching during photosynthetic induction. *Plant Biology*, *2*(2), 161-167. <https://doi.org/10.1055/s-2000-9461>
- Mishra, P., Lohumi, S., Ahmad Khan, H., & Nordon, A. (2020). Close-range hyperspectral imaging of whole plants for digital phenotyping: Recent applications and illumination correction approaches. *Computers and Electronics in Agriculture*, *178*, Article 105780. <https://doi.org/10.1016/j.compag.2020.105780>
- Mishra, P., Polder, G., Gowen, A., Rutledge, D. N., & Roger, J. M. (2020). Utilising variable sorting for normalisation to correct illumination effects in close-range spectral images of potato plants. *Biosystems Engineering*, *197*, 318–323. <https://doi.org/10.1016/j.biosystemseng.2020.07.010>
- Mohd Asaari, M. S., Mishra, P., Mertens, S., Dhondt, S., Inzé, D., Wuyts, N., & Scheunders, P. (2018). Close-range hyperspectral image analysis for the early detection of stress responses in individual plants in a high-throughput phenotyping platform. *ISPRS Journal of Photogrammetry and Remote Sensing*, *138*, 121–138. <https://doi.org/10.1016/j.isprsjprs.2018.02.003>
- Nilsson, H. E. (1995). Remote sensing and image analysis in plant. *Annual Review Phytopathol*, *15*, 489-527.
- Ortaç, G., Bilgi, A. S., Taşdemir, K., & Kalkan, H. (2016). A hyperspectral imaging based control system for quality assessment of dried figs. *Computers and Electronics in Agriculture*, *130*, 38-47. <https://doi.org/10.1016/j.compag.2016.10.001>
- Pandey, P., Ge, Y., Stoerger, V., & Schnable, J. C. (2017). High throughput in vivo analysis of plant leaf chemical properties using hyperspectral imaging. *Frontiers in Plant Science*, *8*, Article 1348. <https://doi.org/10.3389/fpls.2017.01348>
- Ranjan, S., Nayak, D. R., Kumar, K. S., Dash, R., & Majhi, B. (2017). Hyperspectral image classification: A k-means clustering based approach. *2017 4th International Conference on Advanced Computing and Communication Systems (ICACCS)*, 1–7. <https://doi.org/10.1109/ICACCS.2017.8014707>

- Ren, G., Wang, Y., Ning, J., & Zhang, Z. (2020). Using near-infrared hyperspectral imaging with multiple decision tree methods to delineate black tea quality. *Spectrochimica Acta - Part A: Molecular and Biomolecular Spectroscopy*, 237, 118407. <https://doi.org/10.1016/j.saa.2020.118407>
- Sensing, R., Analysis, I., & Plant, I. N. (1995). REMOTE SENSING AND IMAGE ANALYSIS IN PLANT. *Annual Review Phytopathol*, 15, 489–527.
- Shaikh, M. S., Jaferzadeh, K., Thörnberg, B., & Casselgren, J. (2021). Calibration of a hyper-spectral imaging system using a low-cost reference. *Sensors*, 21(11), Article 3738. <https://doi.org/10.3390/s21113738>
- Vigneau, N., Ecarnot, M., Rabatel, G., & Roumet, P. (2011). Potential of field hyperspectral imaging as a non destructive method to assess leaf nitrogen content in Wheat. *Field Crops Research*, 122(1), 25–31. <https://doi.org/10.1016/j.fcr.2011.02.003>
- Vu, H., Tachtatzis, C., Murray, P., Harle, D., Dao, T. K., Le, T. L., Andonovic, I., & Marshall, S. (n.d.). *Rice Seed Varietal Purity Inspection using Hyperspectral Imaging*.
- Witteveen, M., Sterenberg, H. J. C. M., van Leeuwen, T. G., Aalders, M. C. G., Ruers, T. J. M., & Post, A. L. (2022). Comparison of preprocessing techniques to reduce nontissue-related variations in hyperspectral reflectance imaging. *Journal of Biomedical Optics*, 27(10). <https://doi.org/10.1117/1.JBO.27.10.106003>
- Yang, W., Duan, L., Chen, G., Xiong, L., & Liu, Q. (2013). Plant phenomics and high-throughput phenotyping: Accelerating rice functional genomics using multidisciplinary technologies. *Current Opinion in Plant Biology*, 16(2), 180-187. <https://doi.org/10.1016/j.pbi.2013.03.005>
- Zhuang, L., & Ng, M. K. (2020). Hyperspectral mixed noise removal by  $\ell_1$ -norm-based subspace representation. *IEEE Journal of Selected Topics in Applied Earth Observations and Remote Sensing*, 13, 1143-1157. <https://doi.org/10.1109/JSTARS.2020.2979801>

